Tissue nonspecific alkaline phosphatase improves bone quality but does not alleviate craniosynostosis in the FGFR2$^{C342Y/+}$ mouse model of Crouzon syndrome

Hwa Kyung Nam[1#], Sara Dean Schutte[1#], Nan E. Hatch[1*]

[1] Department of Orthodontics and Pediatric Dentistry, School of Dentistry, University of Michigan, Ann Arbor, Michigan, United States of America

* Corresponding author
E-mail: nhatch@umich.edu

[#] These authors contributed equally to this work.

Abstract

Crouzon syndrome is a congenital disorder characterized by craniosynostosis, the premature fusion of cranial bones. Craniosynostosis leads to high intracranial pressure and abnormal skull and facial shapes that are relieved by surgery. Crouzon syndrome is caused by activating mutations in fibroblast growth factor receptor 2 (FGFR2). The goal of this study was to determine if delivery of recombinant tissue nonspecific alkaline phosphatase (TNAP) could prevent or diminish the severity of craniosynostosis in post-natal craniosynostosis onset BALB/c and/or peri-natal craniosynostosis onset C57BL/6 FGFR2$^{C342Y/+}$ mouse models of Crouzon syndrome. Mice were injected with a lentivirus encoding a mineral targeted form of TNAP immediately after birth. Cranial bone fusion as well as cranial bone volume, mineral content and density were assessed by micro computed tomography. Craniofacial shape was measured with calipers using previously established landmarks and measurements. Alkaline phosphatase activity levels were measured in serum. Results show that postnatal delivery of TNAP increases serum levels of alkaline phosphatase activity and improves bone volume, density and mineral content, but does not alleviate craniosynostosis, craniofacial shape or cranial base abnormalities in FGFR2$^{C342Y/+}$ Crouzon mice. These results indicate that post-natal recombinant TNAP enzyme therapy is therapeutic for bone mineralization but not efficacious for relief of FGFR-associated craniosynostosis and associated craniofacial shape defects.

Introduction

Craniosynostosis is the pediatric condition of premature cranial bone fusion. This condition can lead to high intracranial pressure, abnormal skull and facial shapes, blindness, seizures and brain abnormalities [1-6]. Because the sole treatment is surgery, even with appropriately early diagnosis patients can suffer high morbidity [7-9]. Surgical approaches also do not fully correct abnormal skull and facial shapes, which contribute to social challenges. Previous studies showed that the pathogenesis of craniosynostosis can include abnormal boundary formation/maintenance, lineage commitment, proliferation and/or apoptosis of cranial progenitor cells [10-23]. Despite these important advancements, a pharmaceutical treatment for craniosynostosis is not yet realized.

Craniosynostosis occurs in association with activating mutations in *Fgfr2* [10, 12, 24, 25]. Craniosynostosis also occurs at high incidence in infants with hypophosphatasia, a metabolic disorder that occurs due to inactivating mutations in *Alpl*, the gene for tissue nonspecific alkaline phosphatase (TNAP) [26-29]. We previously demonstrated that FGF signaling decreases TNAP expression [14, 30, 31]. TNAP expression is also reduced in primary cells isolated from FGFR2$^{C342Y/+}$ mice that have been induced to differentiate into osteoblasts when cultured *in vitro* or in a 3D collagenous matrix *in vivo* [14, 15]. These results indicate that one of the mechanisms by which FGF signaling influences craniofacial skeletal development may involve reduced TNAP. Notably, postnatal delivery of a recombinant mineral-targeted form of TNAP did prevent craniosynostosis in the TNAP$^{-/-}$ mouse model of hypophosphatasia [32]. The objective of this study was to determine if postnatal delivery of recombinant TNAP could prevent or diminish the severity of craniosynostosis and associated craniofacial shape defects in the FGFR2$^{C342Y/+}$ mouse model of Crouzon syndrome.

Materials and methods

TNAP Lentivirus

Recombinant mineral-targeted TNAP lentivirus was generously provided by Dr. Jose Luis Millán (Sanford Burnham Prebys Medical Discovery Institute, La Jolla, CA). This virus expresses a mineral-targeted protein that is composed of soluble human TNAP enzyme fused to the constant region of human IgG1 and a C-terminal deca-aspartate motif to confer targeting to hydroxyapatite. The aspartate tag confers 30x higher affinity for hydroxyapatite than untagged enzyme [33]. Production and titer of the lentivirus was performed by the University of Michigan Vector Core. Treatment with this recombinant form of TNAP was previously shown to increase serum alkaline phosphatase levels and rescue long bone and craniofacial defects seen in hypophosphatasia [26, 32, 34, 35].

Animal Procedures

Because severity of craniosynostosis and associated craniofacial shape defects are variable on the mixed genetic background, $FGFR2^{C342Y/+}$mice were backcrossed with BALB/c and C57BL/6 mice (obtained from Charles River Laboratories) for at least fifteen generations prior to experiments. BALB/c $FGFR2^{C342Y/+}$mice have a moderate form of Crouzon syndrome with craniosynostosis apparent between three and four weeks after birth [15]. C57BL/6 mice have a severe form of Crouzon syndrome with craniosynostosis first apparent in neonatal mice (data not shown). Genotyping was performed as previously described [12, 15]. Briefly, DNA from tail

digests was amplified by polymerase chain reaction using 5'-gagtaccatgctgactgcatgc-3'and 5'-ggagaggcatctctgtttcaagacc-3' primers to yield a 200 base pair band for wild type FGFR2 and a 300 base pair band for mutant FGFR2^{C342Y}. Mice were fed ad libitum and housed under standard 12 hour dark/light cycles. Litters were randomly assigned to treatment/no treatment groups. Treated mice were injected with 1.0 x 10^7 transforming units lentivirus or an equivalent volume of phosphate buffered saline via the jugular vein two days after birth. BALB/c mice (n=12 FGFR2$^{+/+}$ control mice, n=14 FGFR2$^{C342Y/+}$ control mice, n=16 FGFR2$^{C342Y/+}$ TNAP lentivirus treated mice) were euthanized by CO_2 overdose at four weeks post-natal and C57BL/6 mice (n=7 FGFR2$^{+/+}$ control mice, n=7 FGFR2$^{C342Y/+}$ control mice, n=14 FGFR2$^{C342Y/+}$ TNAP lentivirus treated mice) were euthanized by CO_2 overdose at three weeks post-natal for analyses. BALB/c mice were sacrificed at a later age than C57BL/6 mice because craniosynostosis onset occurs later in BALB/C than in C57BL/6 FGFR2$^{C342Y/+}$ mice. Blood was collected by aortic puncture under surgical anesthesia. Mice were weighed, and body length was measured for each animal. All animal procedures were prospectively approved of by the University of Michigan's University Committee on Use and Care of Animals (UCUCA, protocol PRO00006815). All samples were de-identified as to genotype and treatment group, and each analysis was performed on all BALB/c mice or on all C67BL/6 mice at one time. The primary outcome assessment was craniosynostosis incidence. Secondary outcome assessments included cranial bone density measurements, craniofacial shape measurements, cranial base synchondrosis fusions and cranial base bone lengths.

Serum Analyses

Mice were fasted for six hours prior to blood collection. Alkaline phosphatase activity (AP) in serum was quantified using the colorimetric reagent 4-nitrophenyl-phosphate disodium hexahydrate (Sigma), as compared to a standard curve using commercially available alkaline phosphatase enzyme (Sigma). Inorganic phosphate quantifications were performed using commercially available kits (Pointe Scientific), also as compared to standard curves.

Micro Computed Tomography

Whole skulls were scanned at an 18 µm isotropic voxel resolution using the eXplore Locus SP micro-computed tomography imaging system (GE Healthcare Pre-Clinical Imaging, London, ON, Canada). Regions of interest (ROI's) for parietal and frontal bones were established as 1 mm in length, 1 mm in width and depth equivalent to thickness of bone, as previously described [15, 29]. Density, volume and mineral content of cranial bones from mice were measured using previously established methods using Microview version 2.2 software (GE Healthcare Pre-Clinical Imaging, London, ON) and established algorithms [36, 37].

Cranial Suture Assessment

Fusion between cranial bones (fusion of coronal suture, lambdoid suture and sagittal suture) plus fusion of the inter-sphenoidal (ISS) and spheno-occipital (SOS) synchondroses were identified on micro CT scans of skulls dissected mice. Cranial sutures were viewed using the two-dimensional micro CT slices in an orthogonal view across the entire length of the suture or synchondrosis, as previously described [15, 29].

Reliability of suture fusion assessment was verified by both intra-operator and inter-operator reliability statistics by calculating intraclass correlation coefficients (ICC). Intra-operator reliability statistics was carried out by assessing suture fusion status of the coronal, sagittal and lambdoid sutures as well as the inter-sphenoidal (ISS) and spheno-occipital (SOS) synchondroses on fifteen micro CT scans by one investigator two times separated by a two-month period. Inter-operator reliability was carried out by analyzing fifteen micro CT scans by a second investigator. The ICC for intraoperator reliability for suture fusion assessment is .970 ($p \leq .0001$) and the ICC for interoperator reliability is .972 ($p \leq .0001$). Thus, there is high intraoperator and interoperator reliability for suture fusion assessment.

Linear Measurements

Craniofacial linear skeletal measurements were taken using digital calipers on dissected skulls. Linear measurements were calculated using previously reported craniofacial skeletal landmarks [15, 38, 39], including standard measurements currently in use by the Craniofacial Mutant Mouse Resource of Jackson Laboratory (Bar Harbor, ME). Linear measurements were normalized to total skull length (measured from nasale to opisthion) to account for size differences between $FGFR2^{+/+}$ and $FGFR2^{C342Y/+}$ mice. Measurements were performed twice and an average of the two measurements was utilized for statistical comparison by genotype and treatment. Cranial base anterior-posterior bone lengths were measured on micro CT scans using *Dolphin Imaging 11.0* software (Dolphin Imaging and Management Solutions, Chatsworth, CA), as previously described [40].

Statistics

An Analysis of Variance (ANOVA) was performed to compare groups by gender, genotype and treatment group. Because serum AP levels varied in mice injected with the lentivirus, linear regressions were also performed to determine if, and to what extent serum AP levels associated with changes in measured phenotypes. The incidence of cranial suture fusion, and cranial base synchondrosis fusion was analyzed by the Fishers exact test.

Results

Injection with the TNAP expression lentivirus significantly increased serum alkaline phosphatase (AP) levels in all of the treated mice (Table 1). BALB/c Crouzon mice injected with the lentivirus increased serum AP levels by 1.2 U/mL when compared to control Crouzon mice ($p<.0001$) when measured at four weeks old. C57BL/6 Crouzon mice injected with the TNAP expression lentivirus increased serum AP levels by 1.8 U/mL when compared to control Crouzon mice ($p<.0001$) when measured at three weeks old. No significant difference in serum AP levels were seen between untreated Crouzon and wild type mice on the BALB/c or C57BL/6 backgrounds. As expected, injection with the lentivirus did not alter serum inorganic phosphate (P_i) levels.

Initial statistical comparison of groups by ANOVA showed that Crouzon mice weigh less and are shorter in body length than their wild type littermates, regardless of genetic background (Table 1). Linear regression performed to account for serum AP level variability in the lentivirus injected mice showed that, on the BALB/c background, serum AP levels did not alter weight in

wild type mice but did decrease weight in Crouzon mice by 0.9 g per U/ml which accounted for 37% of the weight variability in in these mice ($p<.03$). On the C57BL/6 background, linear regression showed no impact of serum AP level on weight, regardless of genotype. Serum AP levels did not alter body length, regardless of genetic background or genotype.

Table 1. Serum and Body Measurements in TNAP vs. untreated Balb/C and C57Bl/6mice.

Strain	Genotype	Treatment	Body Weight (g)	Body Length (mm)	Serum AP Level (units/ml)	Serum Pi Level (mg/dl)
Balb/C	$FGFR2^{+/+}$	no	13.5 +/- 2.2*	7.4 +/- 0.3*	0.03 +/- 0.01	10.9 +/- 0.8
Balb/C	$FGFR2^{C342Y/+}$	no	9.2 +/- 1.7	6.5 +/- 0.3	0.03 +/- 0.78	9.9 +/- 1.4
Balb/C	$FGFR2^{C342Y/+}$	yes	8.9 +/- 2.6	6.5 +/- 0.7	1.30 +/- 0.54#	9.8 +/- 1.1
C57Bl/6	$FGFR2^{+/+}$	no	8.7 +/- 0.1*	6.9 +/- 0.3*	0.01 +/- 0.01	9.5 +/- 1.0
C57Bl/6	$FGFR2^{C342Y/+}$	no	5.8 +/- 1.1	5.8 +/- 0.6	0.02 +/- 0.01	8.7 +/- 1.1
C57Bl/6	$FGFR2^{C342Y/+}$	yes	6.6 +/- 1.0	5.9 +/- 0.4	1.93 +/- 0.77#	9.0 +/- 0.6

* p value < 0.01 between genotypes

p value < 0.01 between treatment groups

Qualitative analysis of craniofacial skeletal shape suggested that Crouzon mice differ in morphology from their wild type counterparts, and that post-natal delivery of mineral-targeted TNAP via lentivirus did not impact morphology (Figs 1,2). Craniofacial skeletal linear measurements normalized to total skull length revealed many differences between $FGFR2^{342Y/+}$ Crouzon and $FGFR2^{+/+}$ wild type mice on both congenic backgrounds (Table 2). BALB/c Crouzon mice had increased cranial height, cranial width, inner canthal distance, parietal bone length and cranial height to width ratios, with decreased nasal bone length. C57BL/6 Crouzon mice had increased cranial height, cranial width, inner canthal distance, frontal bone length, parietal bone length and cranial height to width ratios, with decreased nose and nasal bone lengths.

Treatment with the TNAP lentivirus did not alter craniofacial skeletal measurements in Crouzon mice on either genetic background.

Table 2. Linear Craniofacial Skeletal Measurements in TNAP vs. untreated BALB/c and C57Bl/6 mice.

Strain	Measurement	$FGFR2^{+/+}$ vehicle	$FGFR2^{C342Y/+}$ vehicle	$FGFR2^{C342Y/+}$ TNAP
BALB/c	Cranial Height	.36 +/- .01*	.45 +/- .01	.45 +/- .01
BALB/c	Cranial Width	.55 +/- .01*	.63 +/- .01	.62 +/- .01
BALB/c	Inner Canthal Distance	.20 +/- .01*	.25 +/- .01	.26 +/- .01
BALB/c	Nose Length	.65+/- .01	.65 +/- .01	.65 +/- .01
BALB/c	Nasal Bone Length	.33 +/- .02*	.32 +/- .01	.32 +/- .03
BALB/c	Frontal Bone length	.33 +/- .02	.33 +/- .01	.34 +/- .03
BALB/c	Parietal Bone Length	.20 +/- .01*	.25 +/- .02	.26 +/- .01
BALB/c	Ratio Height to Width	.66 +/- .02*	.72 +/- .02	.72 +/- .02
C57Bl/6	Cranial Height	.38 +/- .01*	.52 +/- .01	.52 +/- .03
C57Bl/6	Cranial Width	.55 +/- .01*	.64 +/- .01	.64 +/- .02
C57Bl/6	Inner Canthal Distance	.23 +/- .01*	.29 +/- .01	.29 +/- .01
C57Bl/6	Nose Length	.65 +/- .01*	.62 +/- .01	.63 +/- .03
C57Bl/6	Nasal Bone Length	.32 +/- .01*	.23 +/- .02	.23 +/- .01
C57Bl/6	Frontal Bone length	.35 +/- .01*	.40 +/- .02	.41 +/- .03
C57Bl/6	Parietal Bone Length	.22 +/- .01*	.26 +/- .02	.27 +/- .02
C57Bl/6	Ratio Height to Width	.38 +/- .01*	.52 +/- .01	.52 +/- .03

Measures are reported as normalized to total skull length.
* p value < 0.01 between genotypes
# p value < 0.01 between treatment groups

Analysis of cranial bone fusions revealed high incidences of premature fusion of the coronal and lambdoid sutures in both BALB/c and C57BL/6 Crouzon mice, with no fusions evident in wild type mice (Fig. 3). Although 100% of BALB/c and C57BL/6 Crouzon mice exhibited coronal suture fusion, fusions in BALB/c mice tended to be point fusions as opposed to fusion of approximately 1/3 of the coronal suture in the C57BL/6 C mice. Analysis of cranial base synchondrosis fusions also revealed high incidences of fusion of the inter-sphenoidal

198 synchondrosis (ISS) in both strains of Crouzon mice, with no fusions evident in wild type mice.
199 The incidence of fusion of the spheno-occipital synchondrosis (SOS) was higher in C57BL/6
200 Crouzon mice than BALB/c Crouzon mice, despite the younger age of the C57BL/6 mice. No
201 cranial base fusions were evident in the wild type littermate mice. While some trends, including
202 diminished incidence of lambdoid suture fusion and increased incidence of spheno-occipital
203 synchondrosis (SOS) fusion are seen upon treatment, these differences were not statistically
204 significant. Measurement of cranial base bones demonstrated decreased length of the basis-
205 sphenoid and pre-sphenoid bones in BALB/c and C57BL/6 Crouzon as compared to wild type
206 mice (Table 3). Treatment with TNAP did not increase length of the basis-sphenoid bone in
207 Crouzon mice. Treatment with TNAP did increase length of the pre-sphenoid bone in BALB/c
208 Crouzon mice, but not to the equivalent of sphenoid bone length seen in wild type mice.
209 Together, the data indicates that delivery of mineral-targeted TNAP via lentivirus shortly after
210 birth does not impact cranial bone or cranial base bone fusions in these mice. Treatment with
211 the mineral-targeted TNAP may enhance growth of anterior cranial base bones in the model of
212 more moderate Crouzon syndrome (BALB/c strain), but not to the extent seen in control wild
213 type mice.
214
215
216
217
218
219

Table 3. Cranial base measurments in TNAP vs. untreated Balb/C and C57Bl/6 mice.

Strain	Genotype	Treatment	Basis Occipitus (mm)	Basis Sphenoid (mm)	Pre-Sphenoid (mm)
Balb/C	$FGFR2^{+/+}$	vehicle	3.1 +/- 0.1	2.9 +/- 0.1*	2.5 +/- 0.1*
Balb/C	$FGFR2^{C342Y/+}$	vehicle	2.9 +/- 0.3	2.4 +/- 0.3	1.8 +/- 0.1
Balb/C	$FGFR2^{C342Y/+}$	TNAP	2.9 +/- 0.2	2.5 +/- 0.3	1.9 +/- 0.1#
C57Bl/6	$FGFR2^{+/+}$	vehicle	2.8 +/- 0.2	2.9 +/- 0.2*	2.2 +/- 0.1*
C57Bl/6	$FGFR2^{C342Y/+}$	vehicle	2.8 +/- 0.1	2.7 +/- 0.1	1.7 +/- 0.1
C57Bl/6	$FGFR2^{C342Y/+}$	TNAP	3.0 +/- 0.2	2.6 +/-0.1	1.7 +/- 0.1

* p value < 0.01 between genotypes

p value < 0.01 between treatment groups

Micro CT based analyses of cranial bones demonstrated significantly diminished bone mineral density, tissue mineral content, tissue mineral density and bone volume fraction in frontal bones, plus significantly diminished tissue mineral density and bone volume fraction in parietal bones of Crouzon mice when compared to wild type littermates on both BALB/c and C57BL/6 backgrounds (Table 4). Injection with the TNAP lentivirus significantly increased frontal bone mineral density, tissue mineral content and bone volume fraction, plus parietal bone volume fraction in Crouzon mice on the BALB/c background. Injection with the TNAP lentivirus did not significantly impact any of the cranial bone parameters in Crouzon mice on the C57BL/6 background.

Table 4. Cranial bone volume, density and mineral content in TNAP vs. untreated congenic BALB/c and C57BL/6 mice.

Strain	Genotype	Treatment	Cranial Bone	Bone Mineral Content (mg)	Bone Mineral Density (mg/cc)	Tissue Mineral Content (mg)	Tissue Mineral Density (mg/cc)	Bone Volume Fraction
BALB/c	$FGFR2^{+/+}$	PBS	Frontal	.035 +/- .004	405 +/- 14*	.028 +/- .007*	692 +/- 14*	0.41 +/- .03*
BALB/c	$FGFR2^{C342Y/+}$	PBS	Frontal	.031 +/- .008	361 +/- 63	.020 +/- .006#\	671 +/- 18	0.36 +/- .0
BALB/c	$FGFR2^{C342Y/+}$	TNAP	Frontal	.035 +/- .005	401 +/- 26#	.026 +/- .015#	683 +/- 29	0.42 +/- .06#
BALB/c	$FGFR2^{+/+}$	PBS	Parietal	.034 +/- .004	405 +/- 12	.023 +/- .005	693 +/- 15*	0.43 +/- .03*
BALB/c	$FGFR2^{C342Y/+}$	PBS	Parietal	.031 +/- .007	396 +/- 39	.020 +/- .005	669 +/- 24	0.36 +/- .06
BALB/c	$FGFR2^{C342Y/+}$	TNAP	Parietal	.034 +/- .006	403 +/- 27	.025 +/- .012	691 +/- 36	0.42 +/- .07#
C57BL/6	$FGFR2^{+/+}$	PBS	Frontal	.017 +/- .003	245 +/- 25*	.006 +/- .001*	570 +/- 18*	0.12 +/- .01*
C57BL/6	$FGFR2^{C342Y/+}$	PBS	Frontal	.013 +/- .002	209 +/- 25	.004 +/- .001	519 +/- 26	0.10 +/- .01
C57BL/6	$FGFR2^{C342Y/+}$	TNAP	Frontal	.016 +/- .004	225 +/- 30	.004 +/- .001	553 +/- 40	0.11 +/- .01
C57BL/6	$FGFR2^{+/+}$	PBS	Parietal	.015 +/- .001	237 +/- 19	.005 +/- .001	590 +/- 13*	.121 +/- .023*
C57BL/6	$FGFR2^{C342Y/+}$	PBS	Parietal	.012 +/- .003	217 +/- 18	.004 +/- .001	558 +/- 36	.098 +/- .006
C57BL/6	$FGFR2^{C342Y/+}$	TNAP	Parietal	.013 +/- .004	232 +/- 42	.004 +/- .001	575 +/- 32	.105 +/- .009

* p value < 0.01 between genotypes

p value < 0.01 between treatment groups

Discussion

In this study we sought to determine if treatment with recombinant mineral targeted TNAP could rescue the craniofacial skeletal phenotype of $FGFR2^{C342Y/+}$ Crouzon mice when delivered post-natal with lentivirus. The $FGFR2^{C342Y/+}$ mutation was previously demonstrated to cause ligand independent signaling and is therefore widely considered to be an activating mutation leading to increased FGF signaling [41-44]. We pursued this investigation because we previously demonstrated that FGF signaling diminishes TNAP expression [14, 30, 31], and showed that

TNAP deficiency in mice leads to a similar craniofacial phenotype to that seen in FGFR2$^{C342Y/+}$ Crouzon mice including coronal and lambdoid but not sagittal craniosynostosis, fusion of cranial base synchondroses and abnormal brachycephalic/acrocephalic head shapes [12, 15, 29, 40]. Additionally, in a previous study using archival aliquots of lentivirus expressing the mineral targeted recombinant form of TNAP that resulted in increases in serum AP activity in only a small number of the treated mice, we found statistical differences in the morphology of the inferior skull surface and skull height in treated vs. untreated FGFR2$^{C342Y/+}$ mice [45].

Here we found that post-natal lentiviral delivery of recombinant TNAP rescued cranial bone density, mineral content and volume fraction but not craniosynostosis or craniofacial shape in FGFR2$^{C342Y/+}$ Crouzon mice. Improvement of cranial bone density, mineral content and volume fraction by TNAP treatment in the Crouzon mice is consistent with results showing that recombinant mineral targeted TNAP treatment rescues mineralization of craniofacial and long bones in in the *Alpl*$^{-/-}$ mouse model of infantile HPP and humans with infantile and childhood HPP [32, 34, 46, 47]. Treatment with mineral targeted TNAP via lentivirus did not rescue craniosynostosis or craniofacial shape defects in the Crouzon mice. This result is inconsistent with the rescue of craniosynostosis seen in *Alpl*$^{-/-}$ mice treated with mineral targeted recombinant TNAP protein [32] but is consistent with results in human studies which indicate that post-natal treatment with recombinant TNAP protein does not rescue craniosynostosis [26, 47]. While lentiviral TNAP treatment did not rescue cranial base synchondrosis fusion in the Crouzon mice, length of the pre-sphenoid bone was increased in treated mice on the BALB/c genetic background. This result is consistent with our previous study using archival lots of the lentivirus [45] which suggested changes in inferior skull morphology and may indicate that

286 TNAP can promote cranial base growth in more moderate presentations of Crouzon syndrome
287 to some extent.

288 Lack of rescue of craniosynostosis, cranial base synchondrosis fusions and craniofacial shape
289 abnormalities by lentiviral delivery of mineral targeted TNAP indicates that TNAP is not
290 essential for these characteristics of Crouzon syndrome. This could be due to the fact that TNAP
291 levels are not decreased at all stages in FGFR2$^{C342Y/+}$ mice [44] and is consistent with our finding
292 in this study that serum AP levels are similar in untreated Crouzon and wild type mice. It is also
293 possible that TNAP is simply not efficacious for preventing FGFR-associated cranial bone and
294 cranial base bone fusions, despite being decreased in cranial bone progenitor cells [14, 15].
295 More recently we showed that TNAP regulates expression of FGFR2 and Erk1,2 activity [48].
296 This latter data suggests the alternative hypothesis that FGF and Erk1,2 signaling changes cause
297 craniosynostosis in TNAP deficiency as opposed to TNAP deficiency causing craniosynostosis in
298 Crouzon syndrome.

299

300 Acknowledgments

301 Lentiviral vector encoding the mineral targeted form of TNAP was generously provided by Dr.
302 José Luis Millán (Sanford Burnham Prebys Medical Discovery Institute, Human Genetics
303 Program, San Jose, CA).

304

305

References

1. Flapper WJ, Anderson PJ, Roberts RM, David DJ. Intellectual outcomes following protocol management in Crouzon, Pfeiffer, and Muenke syndromes. J Craniofac Surg. 2009;20(4):1252-5. Epub 2009/07/25. doi: 10.1097/SCS.0b013e3181acdf9a. PubMed PMID: 19625842.
2. McCarthy JG, Warren SM, Bernstein J, Burnett W, Cunningham ML, Edmond JC, et al. Parameters of care for craniosynostosis. Cleft Palate Craniofac J. 2012;49 Suppl:1S-24S. Epub 2011/08/19. doi: 10.1597/11-138. PubMed PMID: 21848431.
3. Morriss-Kay GM, Wilkie AO. Growth of the normal skull vault and its alteration in craniosynostosis: insights from human genetics and experimental studies. J Anat. 2005;207(5):637-53. Epub 2005/11/30. doi: 10.1111/j.1469-7580.2005.00475.x. PubMed PMID: 16313397; PubMed Central PMCID: PMCPMC1571561.
4. Okajima K, Robinson LK, Hart MA, Abuelo DN, Cowan LS, Hasegawa T, et al. Ocular anterior chamber dysgenesis in craniosynostosis syndromes with a fibroblast growth factor receptor 2 mutation. Am J Med Genet. 1999;85(2):160-70. Epub 1999/07/16. PubMed PMID: 10406670.
5. Rasmussen SA, Yazdy MM, Frias JL, Honein MA. Priorities for public health research on craniosynostosis: summary and recommendations from a Centers for Disease Control and Prevention-sponsored meeting. Am J Med Genet A. 2008;146A(2):149-58. Epub 2007/12/15. doi: 10.1002/ajmg.a.32106. PubMed PMID: 18080327.
6. Seruya M, Oh AK, Boyajian MJ, Posnick JC, Keating RF. Treatment for delayed presentation of sagittal synostosis: challenges pertaining to occult intracranial hypertension. J Neurosurg Pediatr. 2011;8(1):40-8. Epub 2011/07/05. doi: 10.3171/2011.4.PEDS1160. PubMed PMID: 21721888.
7. Abe H, Ikota T, Akino M, Kitami K, Tsuru M. Functional prognosis of surgical treatment of craniosynostosis. Childs Nerv Syst. 1985;1(1):53-61. Epub 1985/01/01. PubMed PMID: 3986842.
8. Baird LC, Gonda D, Cohen SR, Evers LH, LeFloch N, Levy ML, et al. Craniofacial reconstruction as a treatment for elevated intracranial pressure. Childs Nerv Syst. 2012;28(3):411-8. Epub 2011/11/10. doi: 10.1007/s00381-011-1615-6. PubMed PMID: 22068642.
9. Renier D, Lajeunie E, Arnaud E, Marchac D. Management of craniosynostoses. Childs Nerv Syst. 2000;16(10-11):645-58. Epub 2001/01/11. doi: 10.1007/s003810000320. PubMed PMID: 11151714.
10. Chen L, Li D, Li C, Engel A, Deng CX. A Ser252Trp [corrected] substitution in mouse fibroblast growth factor receptor 2 (Fgfr2) results in craniosynostosis. Bone. 2003;33(2):169-78. Epub 2003/09/23. PubMed PMID: 14499350.
11. Deckelbaum RA, Holmes G, Zhao Z, Tong C, Basilico C, Loomis CA. Regulation of cranial morphogenesis and cell fate at the neural crest-mesoderm boundary by engrailed 1. Development. 2012;139(7):1346-58. Epub 2012/03/08. doi: 10.1242/dev.076729. PubMed PMID: 22395741; PubMed Central PMCID: PMCPMC3294437.
12. Eswarakumar VP, Horowitz MC, Locklin R, Morriss-Kay GM, Lonai P. A gain-of-function mutation of Fgfr2c demonstrates the roles of this receptor variant in osteogenesis. Proc Natl Acad Sci U S A. 2004;101(34):12555-60. Epub 2004/08/19. doi: 10.1073/pnas.0405031101. PubMed PMID: 15316116; PubMed Central PMCID: PMCPMC515096.

13. Holmes G, Rothschild G, Roy UB, Deng CX, Mansukhani A, Basilico C. Early onset of craniosynostosis in an Apert mouse model reveals critical features of this pathology. Dev Biol. 2009;328(2):273-84. Epub 2009/04/25. doi: 10.1016/j.ydbio.2009.01.026. PubMed PMID: 19389359; PubMed Central PMCID: PMCPMC2674120.

14. Liu J, Kwon TG, Nam HK, Hatch NE. Craniosynostosis-associated Fgfr2(C342Y) mutant bone marrow stromal cells exhibit cell autonomous abnormalities in osteoblast differentiation and bone formation. Biomed Res Int. 2013;2013:292506. Epub 2013/06/14. doi: 10.1155/2013/292506. PubMed PMID: 23762837; PubMed Central PMCID: PMCPMC3665166.

15. Liu J, Nam HK, Wang E, Hatch NE. Further analysis of the Crouzon mouse: effects of the FGFR2(C342Y) mutation are cranial bone-dependent. Calcif Tissue Int. 2013;92(5):451-66. Epub 2013/01/30. doi: 10.1007/s00223-013-9701-2. PubMed PMID: 23358860; PubMed Central PMCID: PMCPMC3631296.

16. McGee-Lawrence ME, Li X, Bledsoe KL, Wu H, Hawse JR, Subramaniam M, et al. Runx2 protein represses Axin2 expression in osteoblasts and is required for craniosynostosis in Axin2-deficient mice. J Biol Chem. 2013;288(8):5291-302. Epub 2013/01/10. doi: 10.1074/jbc.M112.414995. PubMed PMID: 23300083; PubMed Central PMCID: PMCPMC3581413.

17. Merrill AE, Bochukova EG, Brugger SM, Ishii M, Pilz DT, Wall SA, et al. Cell mixing at a neural crest-mesoderm boundary and deficient ephrin-Eph signaling in the pathogenesis of craniosynostosis. Hum Mol Genet. 2006;15(8):1319-28. Epub 2006/03/17. doi: 10.1093/hmg/ddl052. PubMed PMID: 16540516.

18. Miraoui H, Marie PJ. Pivotal role of Twist in skeletal biology and pathology. Gene. 2010;468(1-2):1-7. Epub 2010/08/11. doi: 10.1016/j.gene.2010.07.013. PubMed PMID: 20696219.

19. Rice DP, Connor EC, Veltmaat JM, Lana-Elola E, Veistinen L, Tanimoto Y, et al. Gli3Xt-J/Xt-J mice exhibit lambdoid suture craniosynostosis which results from altered osteoprogenitor proliferation and differentiation. Hum Mol Genet. 2010;19(17):3457-67. Epub 2010/06/24. doi: 10.1093/hmg/ddq258. PubMed PMID: 20570969; PubMed Central PMCID: PMCPMC2916710.

20. Rice DP, Kim HJ, Thesleff I. Apoptosis in murine calvarial bone and suture development. Eur J Oral Sci. 1999;107(4):265-75. Epub 1999/09/01. PubMed PMID: 10467942.

21. Twigg SR, Kan R, Babbs C, Bochukova EG, Robertson SP, Wall SA, et al. Mutations of ephrin-B1 (EFNB1), a marker of tissue boundary formation, cause craniofrontonasal syndrome. Proc Natl Acad Sci U S A. 2004;101(23):8652-7. Epub 2004/05/29. doi: 10.1073/pnas.0402819101. PubMed PMID: 15166289; PubMed Central PMCID: PMCPMC423250.

22. Yousfi M, Lasmoles F, El Ghouzzi V, Marie PJ. Twist haploinsufficiency in Saethre-Chotzen syndrome induces calvarial osteoblast apoptosis due to increased TNFalpha expression and caspase-2 activation. Hum Mol Genet. 2002;11(4):359-69. Epub 2002/02/21. PubMed PMID: 11854168.

23. Zhang X, Carpenter D, Bokui N, Soo C, Miao S, Truong T, et al. Overexpression of Nell-1, a craniosynostosis-associated gene, induces apoptosis in osteoblasts during craniofacial development. J Bone Miner Res. 2003;18(12):2126-34. Epub 2003/12/16. doi: 10.1359/jbmr.2003.18.12.2126. PubMed PMID: 14672347.

389 24. Reardon W, Winter RM, Rutland P, Pulleyn LJ, Jones BM, Malcolm S. Mutations in the
390 fibroblast growth factor receptor 2 gene cause Crouzon syndrome. Nat Genet. 1994;8(1):98-
391 103. Epub 1994/09/01. doi: 10.1038/ng0994-98. PubMed PMID: 7987400.
392 25. Wilkie AO, Slaney SF, Oldridge M, Poole MD, Ashworth GJ, Hockley AD, et al. Apert
393 syndrome results from localized mutations of FGFR2 and is allelic with Crouzon syndrome. Nat
394 Genet. 1995;9(2):165-72. Epub 1995/02/01. doi: 10.1038/ng0295-165. PubMed PMID:
395 7719344.
396 26. Whyte MP, Greenberg CR, Salman NJ, Bober MB, McAlister WH, Wenkert D, et al. Enzyme-
397 replacement therapy in life-threatening hypophosphatasia. N Engl J Med. 2012;366(10):904-13.
398 Epub 2012/03/09. doi: 10.1056/NEJMoa1106173. PubMed PMID: 22397652.
399 27. Collmann H, Mornet E, Gattenlohner S, Beck C, Girschick H. Neurosurgical aspects of
400 childhood hypophosphatasia. Childs Nerv Syst. 2009;25(2):217-23. Epub 2008/09/05. doi:
401 10.1007/s00381-008-0708-3. PubMed PMID: 18769927.
402 28. Fraser D. Hypophosphatasia. Am J Med. 1957;22(5):730-46. Epub 1957/05/01. PubMed
403 PMID: 13410963.
404 29. Liu J, Nam HK, Campbell C, Gasque KC, Millan JL, Hatch NE. Tissue-nonspecific alkaline
405 phosphatase deficiency causes abnormal craniofacial bone development in the Alpl(-/-) mouse
406 model of infantile hypophosphatasia. Bone. 2014;67:81-94. Epub 2014/07/12. doi:
407 10.1016/j.bone.2014.06.040. PubMed PMID: 25014884; PubMed Central PMCID:
408 PMCPMC4149826.
409 30. Hatch NE, Li Y, Franceschi RT. FGF2 stimulation of the pyrophosphate-generating enzyme,
410 PC-1, in pre-osteoblast cells is mediated by RUNX2. J Bone Miner Res. 2009;24(4):652-62. Epub
411 2008/12/04. doi: 10.1359/jbmr.081213. PubMed PMID: 19049325; PubMed Central PMCID:
412 PMCPMC2659512.
413 31. Hatch NE, Nociti F, Swanson E, Bothwell M, Somerman M. FGF2 alters expression of the
414 pyrophosphate/phosphate regulating proteins, PC-1, ANK and TNAP, in the calvarial
415 osteoblastic cell line, MC3T3E1(C4). Connect Tissue Res. 2005;46(4-5):184-92. Epub
416 2006/03/21. doi: 10.1080/03008200500237203. PubMed PMID: 16546821.
417 32. Liu J, Campbell C, Nam HK, Caron A, Yadav MC, Millan JL, et al. Enzyme replacement for
418 craniofacial skeletal defects and craniosynostosis in murine hypophosphatasia. Bone.
419 2015;78:203-11. Epub 2015/05/12. doi: 10.1016/j.bone.2015.05.005. PubMed PMID:
420 25959417; PubMed Central PMCID: PMCPMC4466206.
421 33. Nishioka T, Tomatsu S, Gutierrez MA, Miyamoto K, Trandafirescu GG, Lopez PL, et al.
422 Enhancement of drug delivery to bone: characterization of human tissue-nonspecific alkaline
423 phosphatase tagged with an acidic oligopeptide. Mol Genet Metab. 2006;88(3):244-55. Epub
424 2006/04/18. doi: 10.1016/j.ymgme.2006.02.012. PubMed PMID: 16616566; PubMed Central
425 PMCID: PMCPMC2587042.
426 34. Millan JL, Narisawa S, Lemire I, Loisel TP, Boileau G, Leonard P, et al. Enzyme replacement
427 therapy for murine hypophosphatasia. J Bone Miner Res. 2008;23(6):777-87. Epub 2007/12/19.
428 doi: 10.1359/jbmr.071213. PubMed PMID: 18086009; PubMed Central PMCID:
429 PMCPMC2652241.
430 35. Yadav MC, Lemire I, Leonard P, Boileau G, Blond L, Beliveau M, et al. Dose response of
431 bone-targeted enzyme replacement for murine hypophosphatasia. Bone. 2011;49(2):250-6.

Epub 2011/04/05. doi: 10.1016/j.bone.2011.03.770. PubMed PMID: 21458605; PubMed Central PMCID: PMCPMC3117961.

36. Meganck JA, Kozloff KM, Thornton MM, Broski SM, Goldstein SA. Beam hardening artifacts in micro-computed tomography scanning can be reduced by X-ray beam filtration and the resulting images can be used to accurately measure BMD. Bone. 2009;45(6):1104-16. Epub 2009/08/05. doi: 10.1016/j.bone.2009.07.078. PubMed PMID: 19651256; PubMed Central PMCID: PMCPMC2783193.

37. Umoh JU, Sampaio AV, Welch I, Pitelka V, Goldberg HA, Underhill TM, et al. In vivo micro-CT analysis of bone remodeling in a rat calvarial defect model. Phys Med Biol. 2009;54(7):2147-61. Epub 2009/03/17. doi: 10.1088/0031-9155/54/7/020. PubMed PMID: 19287088.

38. Perlyn CA, DeLeon VB, Babbs C, Govier D, Burell L, Darvann T, et al. The craniofacial phenotype of the Crouzon mouse: analysis of a model for syndromic craniosynostosis using three-dimensional MicroCT. Cleft Palate Craniofac J. 2006;43(6):740-8. Epub 2006/11/16. doi: 10.1597/05-212. PubMed PMID: 17105336.

39. Richtsmeier JT, Baxter LL, Reeves RH. Parallels of craniofacial maldevelopment in Down syndrome and Ts65Dn mice. Dev Dyn. 2000;217(2):137-45. Epub 2000/03/08. doi: 10.1002/(SICI)1097-0177(200002)217:2<137::AID-DVDY1>3.0.CO;2-N. PubMed PMID: 10706138.

40. Nam HK, Sharma M, Liu J, Hatch NE. Tissue Nonspecific Alkaline Phosphatase (TNAP) Regulates Cranial Base Growth and Synchondrosis Maturation. Front Physiol. 2017;8:161. Epub 2017/04/06. doi: 10.3389/fphys.2017.00161. PubMed PMID: 28377728; PubMed Central PMCID: PMCPMC5359511.

41. Galvin BD, Hart KC, Meyer AN, Webster MK, Donoghue DJ. Constitutive receptor activation by Crouzon syndrome mutations in fibroblast growth factor receptor (FGFR)2 and FGFR2/Neu chimeras. Proc Natl Acad Sci U S A. 1996;93(15):7894-9. Epub 1996/07/23. PubMed PMID: 8755573; PubMed Central PMCID: PMCPMC38845.

42. Neilson KM, Friesel RE. Constitutive activation of fibroblast growth factor receptor-2 by a point mutation associated with Crouzon syndrome. J Biol Chem. 1995;270(44):26037-40. Epub 1995/11/03. PubMed PMID: 7592798.

43. Robertson SC, Meyer AN, Hart KC, Galvin BD, Webster MK, Donoghue DJ. Activating mutations in the extracellular domain of the fibroblast growth factor receptor 2 function by disruption of the disulfide bond in the third immunoglobulin-like domain. Proc Natl Acad Sci U S A. 1998;95(8):4567-72. Epub 1998/05/16. PubMed PMID: 9539778; PubMed Central PMCID: PMCPMC22530.

44. Pfaff MJ, Xue K, Li L, Horowitz MC, Steinbacher DM, Eswarakumar JVP. FGFR2c-mediated ERK-MAPK activity regulates coronal suture development. Dev Biol. 2016;415(2):242-50. Epub 2016/04/02. doi: 10.1016/j.ydbio.2016.03.026. PubMed PMID: 27034231; PubMed Central PMCID: PMCPMC5580088.

45. Wang E, Nam HK, Liu J, Hatch NE. The effects of tissue-non-specific alkaline phosphatase gene therapy on craniosynostosis and craniofacial morphology in the FGFR2C342Y/+ mouse model of Crouzon craniosynostosis. Orthod Craniofac Res. 2015;18 Suppl 1:196-206. Epub 2015/04/14. doi: 10.1111/ocr.12080. PubMed PMID: 25865549; PubMed Central PMCID: PMCPMC4396711.

475 46. Yamamoto S, Orimo H, Matsumoto T, Iijima O, Narisawa S, Maeda T, et al. Prolonged
476 survival and phenotypic correction of Akp2(-/-) hypophosphatasia mice by lentiviral gene
477 therapy. J Bone Miner Res. 2011;26(1):135-42. Epub 2010/08/06. doi: 10.1002/jbmr.201.
478 PubMed PMID: 20687159; PubMed Central PMCID: PMCPMC3179312.
479 47. Whyte MP, Simmons JH, Moseley S, Fujita KP, Bishop N, Salman NJ, et al. Asfotase alfa for
480 infants and young children with hypophosphatasia: 7 year outcomes of a single-arm, open-
481 label, phase 2 extension trial. Lancet Diabetes Endocrinol. 2018. Epub 2018/12/19. doi:
482 10.1016/S2213-8587(18)30307-3. PubMed PMID: 30558909.
483 48. Nam HK, Vesela I, Siismets E, Hatch NE. Tissue nonspecific alkaline phosphatase promotes
484 calvarial progenitor cell cycle progression and cytokinesis via Erk1,2. Bone. 2018;120:125-36.
485 Epub 2018/10/21. doi: 10.1016/j.bone.2018.10.013. PubMed PMID: 30342227.
486

487

488 **Figure Legends:**

489

490 **Figure 1. Micro CT images of BALB/c congenic untreated and treated FGFR2$^{C342Y/+}$ mice.** Micro
491 CT isosurface images of P28 FGFR2$^{C342Y/+}$ Crouzon (CZ) and wild type (WT) mice on the BALB/c
492 congenic background are shown in axial view from above (A,B,C) and lateral view (B,D,F).
493 Darker bone is bone of diminished density.

494

495 **Figure 2. Micro CT images of C57BL/6 congenic untreated and treated FGFR2$^{C342Y/+}$ mice.** Micro
496 CT isosurface images of P21 FGFR2$^{C342Y/+}$ Crouzon (CZ) and wild type (WT) mice on the C57BL/6
497 congenic background are shown in axial view from above (A,B,C) and lateral view (B,D,F).
498 Darker bone is bone of diminished density. Cranial bone density is diminished in C57BL/6
499 FGFR2$^{C342Y/+}$ mice to the extent that cranial base bones show through the translucent cranial
500 bones.

501

Figure 3. Incidence of craniosynostosis and cranial base synchondrosis fusions in untreated and treated FGFR2$^{C342Y/+}$ mice. No fusions are evident in wild type mice on either the BALB/c or C57BL/6 backgrounds. A high incidence of coronal and lamboid suture fusion but no fusion of the sagittal suture is evident in Crouzon mice on both the BALB/c and C57BL/6 backgrounds. A high incidence of intersphenoidal synchondrosis (ISS) is seen in Crouzon mice on both backgrounds. Spheno-occipital synchondronsis (SOS) is seen approximately half of C57BL/6 Crouzon mice but rarely in BALB/c Crouzon mice. Treatment with TNAP does not significantly influence fusion of any cranial suture or cranial base synchondroses on either genetic background.

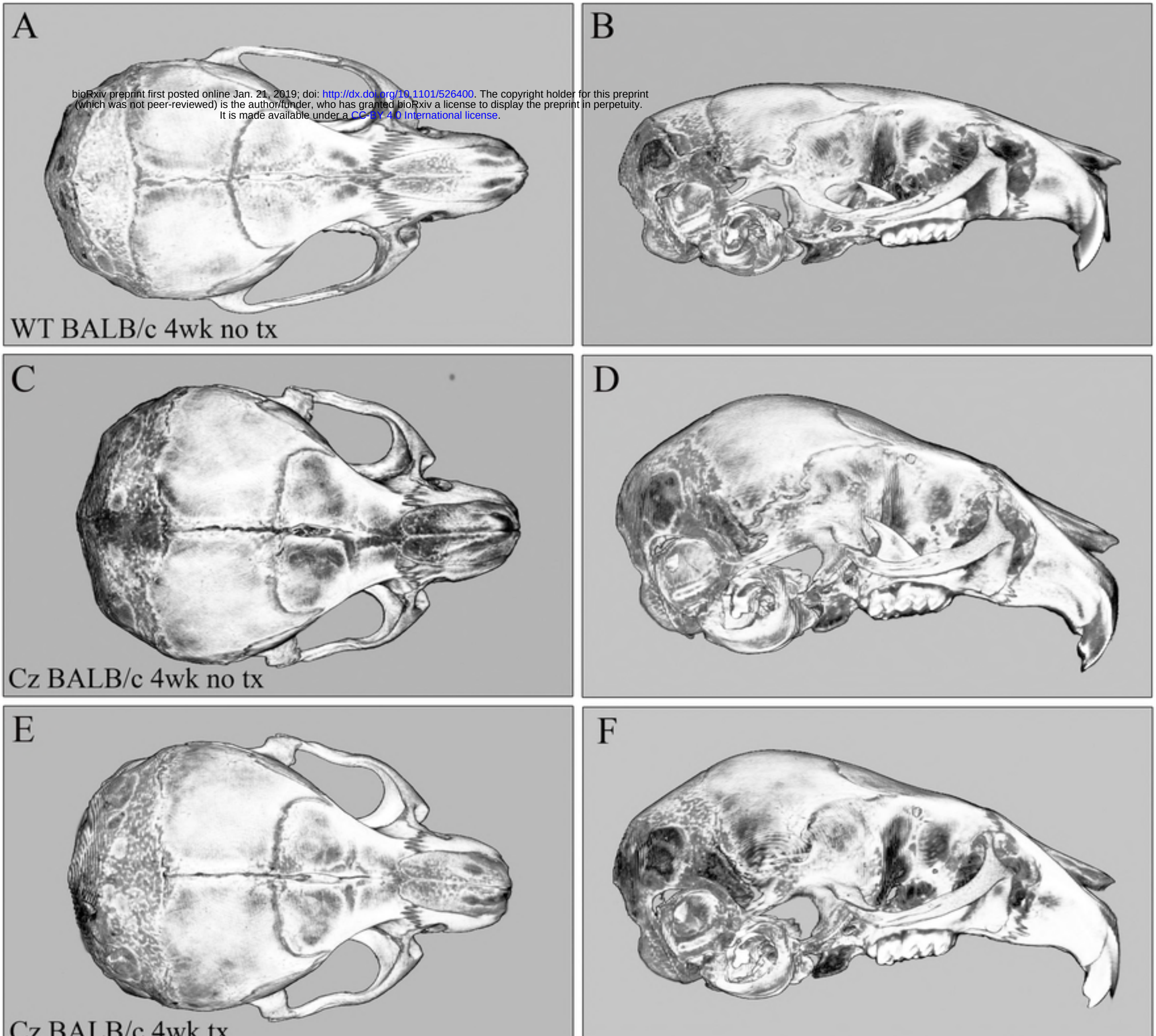

Figure 1. Micro CT images of BALB/c congenic untreated and trea

Figure 2. Micro CT images of C57BL/6 congenic untreated and tr

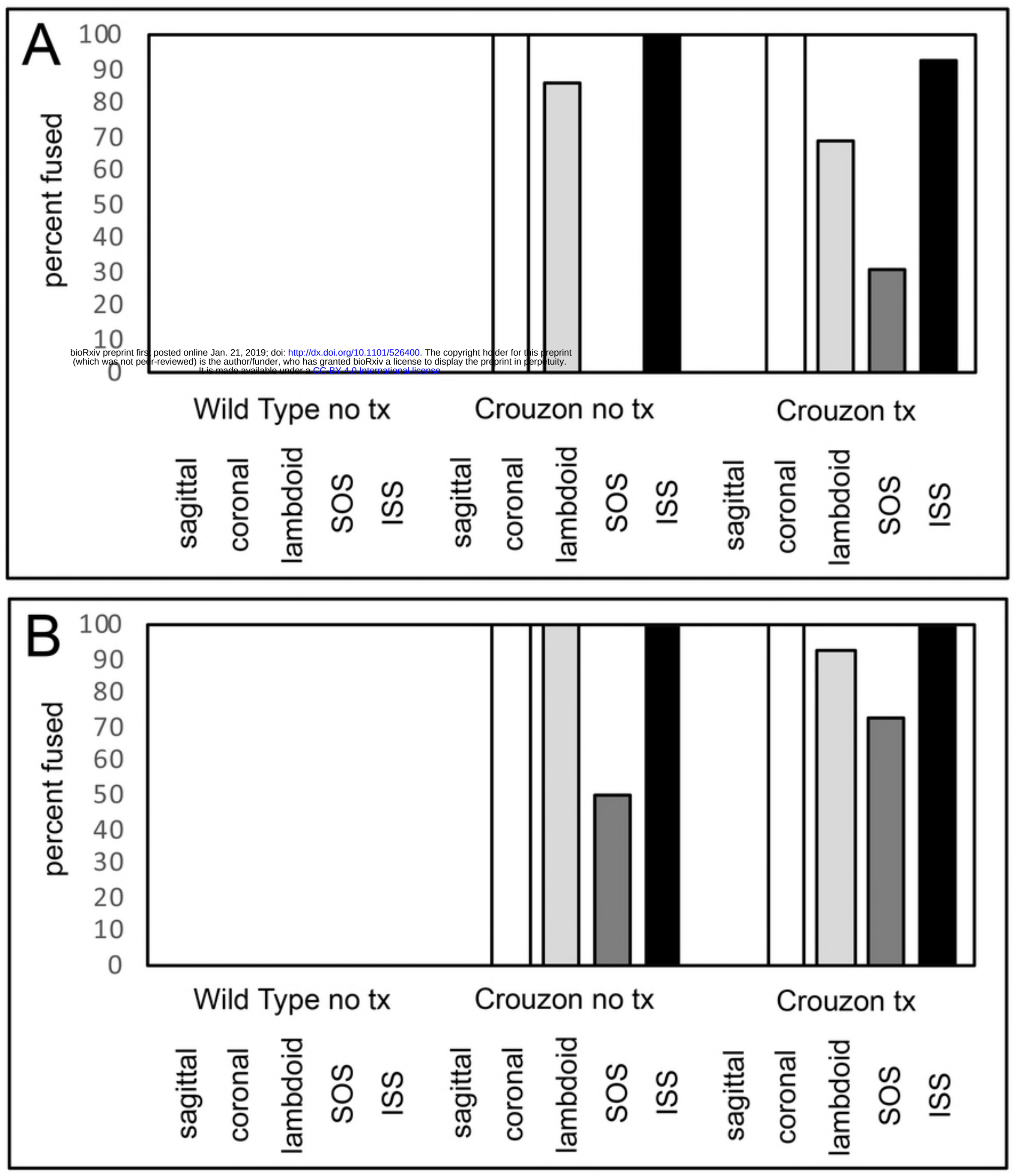

Figure 3. Incidence of craniosynostosis and cranial base synchon